Title

Strain- and thickness-dependent magnetic properties of epitaxial La0.67Sr0.33CoO3/La0.67Sr0.33MnO3 bilayers

Journal

Journal of Applied Physics, 132(19)

ISSN

0021-8979

Authors

Feng, Mingzhen
Ahlm, Nolan J
Kane, Alexander M
et al.

Publication Date

2022-11-21

DOI

10.1063/5.0122009

Peer reviewed

Journal of Applied Physics

Strain- and thickness-dependent magnetic properties of epitaxial $La_{0.67}Sr_{0.33}CoO_3$/$La_{0.67}Sr_{0.33}MnO_3$ bilayers

Cite as: J. Appl. Phys. **132**, 195301 (2022); https://doi.org/10.1063/5.0122009
Submitted: 21 August 2022 • Accepted: 25 October 2022 • Published Online: 15 November 2022

Mingzhen Feng, Nolan J. Ahlm, Alexander M. Kane, et al.

Journal of Applied Physics ARTICLE scitation.org/journal/jap

Strain- and thickness-dependent magnetic properties of epitaxial $La_{0.67}Sr_{0.33}CoO_3$/$La_{0.67}Sr_{0.33}MnO_3$ bilayers

Cite as: J. Appl. Phys. **132**, 195301 (2022); doi: 10.1063/5.0122009
Submitted: 21 August 2022 · Accepted: 25 October 2022 ·
Published Online: 15 November 2022

Mingzhen Feng,[1] Nolan J. Ahlm,[1] Alexander M. Kane,[1] I-Ting Chiu,[2] Dayne Y. Sasaki,[1] Padraic Shafer,[3] Alpha T. N'Diaye,[3] Apurva Mehta,[4] and Yayoi Takamura[1,a)]

AFFILIATIONS

[1]Department of Materials Science and Engineering, University of California, Davis, California 95616, USA
[2]Department of Chemical Engineering, University of California, Davis, California 95616, USA
[3]Advanced Light Source, Lawrence Berkeley National Laboratory, Berkeley, California 94720, USA
[4]Stanford Synchrotron Radiation Lightsource, SLAC National Accelerator Laboratory, Menlo Park, California 94025, USA

Note: This paper is part of the Special Collection Recognizing Women in Applied Physics.
[a)]**Author to whom correspondence should be addressed:** ytakamura@ucdavis.edu

ABSTRACT

Magnetic properties and interfacial phenomena of epitaxial perovskite oxides depend sensitively on parameters such as film thickness and strain state. In this work, epitaxial $La_{0.67}Sr_{0.33}CoO_3$ (LSCO)/$La_{0.67}Sr_{0.33}MnO_3$ (LSMO) bilayers were grown on $NdGaO_3$ (NGO) and $LaAlO_3$ (LAO) substrates with a fixed LSMO thickness of 6 nm, and LSCO thickness (t_{LSCO}) varying from 2 to 10 nm. Soft x-ray magnetic spectroscopy revealed that magnetically active Co^{2+} ions that strongly coupled to the LSMO layer were observed below a critical t_{LSCO} for bilayers grown on both substrates. On LAO substrates, this critical thickness was 2 nm, above which the formation of Co^{2+} ions was quickly suppressed leaving only a soft LSCO layer with mixed valence Co^{3+}/Co^{4+} ions. The magnetic properties of both LSCO and LSMO layers displayed strong t_{LSCO} dependence. This critical t_{LSCO} increased to 4 nm on NGO substrates, and the magnetic properties of only the LSCO layer displayed t_{LSCO} dependence. A non-magnetic layer characterized by Co^{3+} ions and with a thickness below 2 nm exists at the LSCO/substrate interface for both substrates. The results contribute to the understanding of interfacial exchange spring behavior needed for applications in next generation spintronic and magnetic memory devices.

I. INTRODUCTION

Over the past few decades, extensive research has been conducted on transition-metal oxides with the ABO_3 perovskite structure due to their fascinating electronic and magnetic properties, such as metal–insulator transitions, colossal magnetoresistance, and superconductivity.[1–3] This rich behavior arises due to interactions between the charge, orbital, spin, and lattice degrees of freedom.[4] In epitaxial thin films, lattice strain and interfacial phenomena greatly differ from those in bulk materials. Thus, tuning these parameters can be effective means to modify the electronic and magnetic properties, as well as lead to emergent phenomena which can be harnessed for next generation spintronic devices and magnetic random access memory.[5–12] For example, when ferromagnetic (FM) $La_{0.5}Sr_{0.5}CoO_3$ thin films (thickness < 30 nm) are grown under compressive strain on $LaAlO_3$ (LAO) substrates, they demonstrate an enhancement of the Curie temperature (T_c) by ~50 K compared to thin films grown under tensile strain on $SrTiO_3$ (STO) substrates. In another work, Liao *et al.* demonstrated that the magnetic easy axis of FM LSMO thin films grown on (110)-oriented $NdGaO_3$ (NGO) substrates could be rotated in the film plane by an angle of 90° by the insertion of one unit cell of a STO buffer layer. It is believed that this effect results from the coupling of the BO_6 octahedra across the interfaces of this heterostructure.[12] In addition, Kan *et al.* demonstrated that magnetic anisotropy can be tuned by controlling the oxygen coordination environment at $SrRuO_3$/$Ca_{0.5}Sr_{0.5}TiO_3$ interfaces.[13] The Ru–O–Ti

bond angle between the corner-shared TiO_6 and RuO_6 octahedra at the interface increased as the number of $Ca_{0.5}Sr_{0.5}TiO_3$ monolayers increased, thereby resulting in a monoclinic-to-tetragonal structural transition in the $SrRuO_3$ layer.

Interfacial phenomena have also been investigated in an all-perovskite exchange spring system composed of LSCO and LSMO layers with large and small coercivities, respectively.[10,14–17] Soft x-ray magnetic spectroscopy showed that the LSCO/LSMO interface was characterized by magnetically active Co^{2+} ions, which coupled magnetically to the soft FM LSMO layer.[14] For LSCO thicknesses of <5 nm, the hysteresis loops showed only a single magnetic switching event, despite being composed of two chemically distinct layers. As the LSCO thickness (t_{LSCO}) increased, the concentration of Co^{2+} ions in the interfacial layer gradually decreased[16] and a hard LSCO layer formed below it. As a result, exchange spring behavior was observed where the hard LSCO layer biased the composite soft layer, leading to a horizontal shift of the hysteresis loops in a direction opposite of the original biasing field.[14,15] In this case, the hard/soft magnetic interface existed within the LSCO layer rather than at the LSCO/LSMO chemical interface. Such unique exchange coupling behavior provides potential applications in next generation spintronic and magnetic memory devices. In this prior work, the bilayers were grown on $(LaAlO_3)_{0.3}(Sr_2AlTaO_6)_{0.7}$ (LSAT) substrates with an $a^0a^0a^0$ tilt pattern[8] where both layers exist under minimal lattice strain ($\varepsilon_{LSCO} = 0.9\%$, $\varepsilon_{LSMO} = -0.2\%$),[15] where the biaxial strain was defined as $\varepsilon = (a_{strained} - a_{bulk})/a_{bulk}$. While the effect of lattice strain on perovskite oxide thin films has been studied systematically as a function of parameters such as film thickness and magnitude/sign of lattice mismatch,[6–12] the impact of strain and octahedral tilts on interfacial phenomena in heterostructures such as the LSCO/LSMO system remains largely unexplored.

In this work, epitaxial LSCO/LSMO bilayers were grown on two different substrates, (110)-oriented NGO and (001)-orientated LAO substrates. NGO has an orthorhombic (o) symmetry with the $a^-a^-c^+$ tilt pattern in a Glazer notation.[18] The (110)-oriented NGO substrate can be redefined as a pseudocubic (pc) unit cell with a slightly rectangular in-plane lattice ($a_{pc} = 3.855$ Å, $b_{pc} = 3.863$ Å) and $c_{pc} = 3.855$ Å at room temperature using a $(110)_O \parallel (001)_{pc}$ and $(002)_O \parallel (100)_{pc}$ transformation.[19] Thus, this growth surface shares similar lattice constants with a (001)-oriented LSAT substrate ($a = b = c = 3.868$ Å) but offers a different octahedral tilt pattern from our previous studies.[14–17] In contrast, LAO has a rhombohedral structure with the $a^-a^-a^-$ tilt pattern and $a_{pc} = 3.791$ Å at room temperature.[20] The LSCO layer exists under in-plane tensile strain (0.7%) on NGO substrates but experiences compressive strain (−1.0%) on LAO substrates. In contrast, the LSMO layer is nearly un-strained (−0.1%) on NGO substrates but experiences a large compressive strain (−2.0%) on LAO substrates. Both LSCO and LSMO share the same rhombohedral $a^-a^-a^-$ tilt pattern as LAO,[8,10,21] however, the lattice mismatch between the film and substrate can lead to a tetragonal distortion of the pseudocubic unit cell, as well as alter the octahedral tilt patterns observed in the films. The resulting structural differences in the LSCO/LSMO bilayers lead to notable differences in their magnetic spin/electronic structures and bulk magnetic properties. For bilayers grown on both substrates, a non-magnetic layer characterized by Co^{3+} ions existed at the LSCO/substrate interface with a thickness below 2 nm. Above this layer, magnetically active Co^{2+} ions that strongly couple to the LSMO layer were observed below a critical LSCO thickness. This critical thickness was 2 and 4 nm for bilayers on LAO and NGO substrates, respectively. Above this critical thickness, the LSCO layers on LAO substrates were characterized by mixed Co^{3+}/Co^{4+} ions with soft FM properties, and both LSMO and LSCO layers displayed a strong LSCO thickness dependence. In contrast, when grown on NGO substrates, a hard FM LSCO layer was observed with mixed Co^{3+}/Co^{4+} ions and only the magnetic properties of the LSCO layer varied with LSCO thickness. These results enable us to develop a deeper understanding of the interconnected strain- and thickness-dependent magnetic and electronic properties at perovskite oxide interfaces.

II. EXPERIMENTAL METHODS

Epitaxial LSCO/LSMO bilayers were deposited by pulsed laser deposition on (110)-oriented NGO and (001)-oriented LAO substrates. All layers were grown using a KrF excimer laser ($\lambda = 248$ nm), with 1.0 J/cm^2 laser energy, and 1 Hz laser repetition rate. The substrate temperature was held at 700 °C and the oxygen pressure was 0.3 Torr. Samples were slowly cooled to room temperature in 300 Torr O_2 to ensure proper oxygen stoichiometry. The LSCO layers were grown first directly on the substrate with varying thickness, and the topmost LSMO layers had a fixed thickness of 6 nm. The growth order was determined based on our previous study that showed that no exchange spring behavior existed when the LSMO layer was grown first, due to the quick accommodation of epitaxial strain in the LSMO sublayer.[10] Bilayers grown on NGO substrates are referred to as samples CxM6-N (x = 2–10, referring to the LSCO layer thickness in nm) and similarly, bilayers grown on LAO substrates are referred to as samples CxM6-L. Reference samples of a single-layer LSMO thin film with 6 nm thickness and LSCO thin films with thicknesses ranging from 2 to 10 nm were grown on both substrates.

Structural characterization was performed using resonant x-ray reflectivity (RXRR) at Beamline 2-1 of the Stanford Synchrotron Radiation Lightsource (SSRL) and high-resolution x-ray diffraction (XRD) using a Bruker D8 Discover 4-circle diffractometer. RXRR measurements were carried out at 8000 eV, as well as the Co K-edge (7723 eV) and Mn K-edge (6553 eV). The transition metal K-edge energies were determined by performing Kramers–Kronig transformations on the x-ray absorption near edge structure energy spectra and correspond to energies where the real part of atomic scattering factor, f'', is a minimum. As a result, the RXRR spectra have increased sensitivity to the chemical contrast between all the deposited layers and substrates which have similar densities.[22] An off-resonant measurement with 8000 eV was also taken due to the similar energy to Cu-K_α x rays which are widely used in laboratory diffractometers. The thickness, roughness, and density of each layer was determined by fitting the RXRR profiles using GenX software,[23] and the strain states of the layers were obtained by reciprocal space maps (RSM) and by fitting the XRD curves using Leptos software.[24]

Bulk magnetic properties were investigated at 80 K using the vibrating sample magnetometer (VSM) of a Quantum Design

VersaLab system. The magnetic field was applied along the in-plane $[100]_{pc}$ direction for samples on LAO substrates and along the in-plane $[001]_o$ direction for samples on NGO substrates. The diamagnetic background from the LAO substrates and large paramagnetic background from the NGO substrates were subtracted from the raw data. The magnetization of the bilayers was normalized by the surface area and reported as areal magnetization (emu/cm^2). Soft x-ray absorption (XA) and x-ray magnetic circular dichroism (XMCD) spectra were acquired at the Co and Mn L-edges at 80 K using Beamline 4.0.2 of the Advanced Light Source (ALS) in total electron yield (TEY) and luminescence yield (LY) modes. Due to the finite escape depth of secondary electrons, the TEY mode is most sensitive to the top 5–10 nm of the sample surface, and therefore probes the entire LSMO layer and only the LSCO layer at the LSCO/LSMO interface.[25] In contrast, the LY mode detects the conversion of x rays into visible light in the substrate after transmitting through the entire LSCO and LSMO layers, and thus provides the averaged information through the whole film thickness.[26] XMCD spectra were calculated as the difference between two jointly normalized XA spectra collected with right (I_{RCP}) and left (I_{LCP}) circularly polarized x rays.[27] Specifically, I_{RCP} and I_{LCP} were scaled by a constant value (α) so that their averaged spectrum spans the range of 0–1; then XMCD intensities were calculated as $\alpha(I_{RCP} - I_{LCP})$. Note that this convention yields XMCD intensity values ~2 times that of asymmetry values calculated as $(I_{RCP} - I_{LCP})/(I_{RCP} + I_{LCP})$. In these measurements, a 0.3 T magnetic field was applied parallel to the incident x-ray beam which was 60° from the surface normal with its in-plane projection parallel to the $[100]_{pc}$ direction for bilayers on LAO substrates and along the in-plane $[001]_o$ direction for bilayers on NGO substrates. It should be noted that for bilayers grown on NGO substrates, the Co- and Mn-edge XMCD LY spectra are not reported due to the extremely low luminescence yield.[28]

III. RESUTLS AND DISCUSSION

A. Structural characterization

Figure 1(a) shows the RXRR curves for bilayer C8M6-L as an example and Table I lists the parameters derived from the best fits. The three spectra were fit simultaneously to one structural model. A thin carbon capping layer was added to the fitting model due to sample exposure to x rays in air. The layer thickness, roughness, and scattering length density (SLD) were determined by fitting the RXRR spectra using the GenX program. These best fits indicate that the LSMO and LSCO layers are better represented as two distinct layers which sum to the expected total thicknesses. The interface/surface layers have slightly lower density than the main layers and the interfacial roughness is below 6 Å. The fitting results agree with our previous studies on LSCO/LSMO bilayers.[14,16,17] Figures 1(b) and 1(c) show RSMs around the $(103)_{pc}$ reflections for the two thickest bilayers, C10M6-L and C10M6-N. The film and substrate peaks are vertically aligned, indicating that the films are fully strained on both substrates. The two LAO substrate peaks in Fig. 1(b) indicate the twin structure[29] of the LAO substrate. The film peaks of LSCO and LSMO are marked with the red dotted circle.

Figures 2(a) and 2(b) show XRD ω–2θ scans taken around the $(002)_{pc}$ LAO and $(220)_o$ NGO substrate peaks, respectively. Due to the twin structure[29] of the LAO substrate, the overall film quality is slightly degraded compared to the bilayers grown on the NGO substrates. With the pseudocubic transformation, the NGO $(220)_o$ peak corresponds to a $(002)_{pc}$ peak. LSCO and LSMO layers are under compressive strain on LAO substrates, therefore, both layers appear at lower 2θ angles compared to the substrate peak. On NGO substrates, the LSMO layer exists under compressive strain, while the LSCO layer is under tensile stain, so the film peaks appear on either side of the NGO substrate peak. Due to the overlap between the two film peaks and the substrate peak, it is

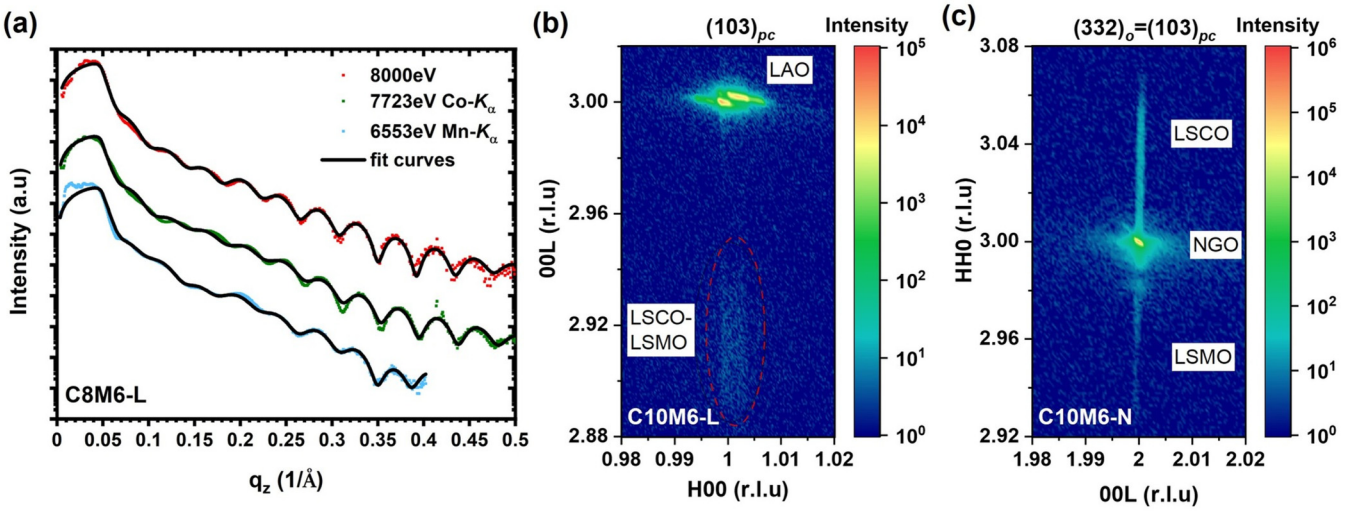

FIG. 1. (a) RXRR spectra for bilayer C8M6-L. Colored symbols are experimental data and black curves are fits corresponding to the parameters listed in Table I. RSMs for bilayer C10M6 on (b) LAO substrates (film peaks are marked with the red dotted circle) and (c) NGO substrates around the $(103)_{pc}$ reflections.

TABLE I. Fit parameters for XRR spectra for bilayer C8M6-L.

Layer	Thickness (nm)	Roughness (nm)	Co-edge SLD (10^{-6} Å^{-2})	Mn-edge SLD (10^{-6} Å^{-2})
Carbon layer	2.38	0.52	11-0.008i	9-0.1i
LSMO surface	2.41	0.54	47-4i	42-5i
LSMO	3.95	0.39	47-4i	44-5i
LSCO interface	3.13	0.57	47-4i	49-4i
LSCO	5.14	0.50	48-5i	50-5i
LAO	…	1.38	As bulk	As bulk

difficult to denote clear film peak positions and thus the full ω–2θ scans were fit using Leptos software.[24] The fit curves are shown in black and the calculated *c/a* ratios are plotted in the insets. The fitting results show that the tetragonal distortion (quantified as *c/a* ratios) for the LSCO and LSMO layers on LAO substrates are $(c/a)_{LSCO} = 1.03$ and $(c/a)_{LSMO} = 1.05$, respectively, and neither change appreciably with LSCO thickness. This $(c/a)_{LSMO}$ value is in good agreement with the literature data for a single-layer LSMO film on LAO substrates.[30] On NGO substrates, $(c/a)_{LSMO}$ varies between 1.01 and 1.015, which is slightly larger than the value reported for a single-layer LSMO film [$(c/a)_{LSMO} = 1.005$[30] and 1.01[7]]. This result suggests that the presence of both the NGO substrate and the underlying LSCO layer affects the octahedral tilt pattern/angles and tetragonal distortion of the LSMO layer.[10]

For the LSCO layer, the $(c/a)_{LSCO}$ value for the thicker bilayers matches well with that of a single-layer LSCO film, and a trend of lattice expansion is observed for the thinner bilayers.

B. Bulk magnetic properties

The magnetic properties of the LSCO/LSMO bilayers with varying LSCO thickness grown on LAO and NGO substrates are plotted in Figs. 3(a) and 3(b). All bilayers on LAO substrates [Fig. 3(a)] do not show distinct magnetic switching events despite the fact that distinct chemical layers were confirmed by the XRD and RXRR measurements. It should be noted that VSM bulk magnetic hysteresis loops may not clearly distinguish between two FM layers switching independently with similar coercivity. Starting with bilayer C4M6-L, the coercive field (H_c) of the bilayers gradually increases with increasing LSCO layer thickness (0.073 T for bilayer C2M6-L, 0.025 T for bilayer C4M6-L, 0.061 T for bilayer C8M6-L, 0.078 T for bilayer C10M6-L). These H_c values are smaller than single-layer LSCO films on LAO substrates (0.03 T for C4-L, 0.14 T for C8-L and 0.16 T for C10-L) and slightly larger than the single-layer LSMO film (0.013 T for M6-L) [see Fig. S1 in the supplementary material]. The areal saturation magnetization (M_s) [see Fig. S2(a) in the supplementary material] as well as the loop squareness (defined as remanent magnetization, M_r, divided by M_s) for the thicker bilayers increase with LSCO thickness, though these increases are not systematic [see Fig. S2(b) in the supplementary material]. Bilayer C2M6-L is an outlier with an areal M_s similar to that of bilayer C10M6-L despite its smaller LSCO thickness, suggesting a higher magnetic moment of its FM ions. Furthermore, the C10M6-L hysteresis loop shows an additional hard phase component compared to bilayer C2M6-L despite their similar H_c values.

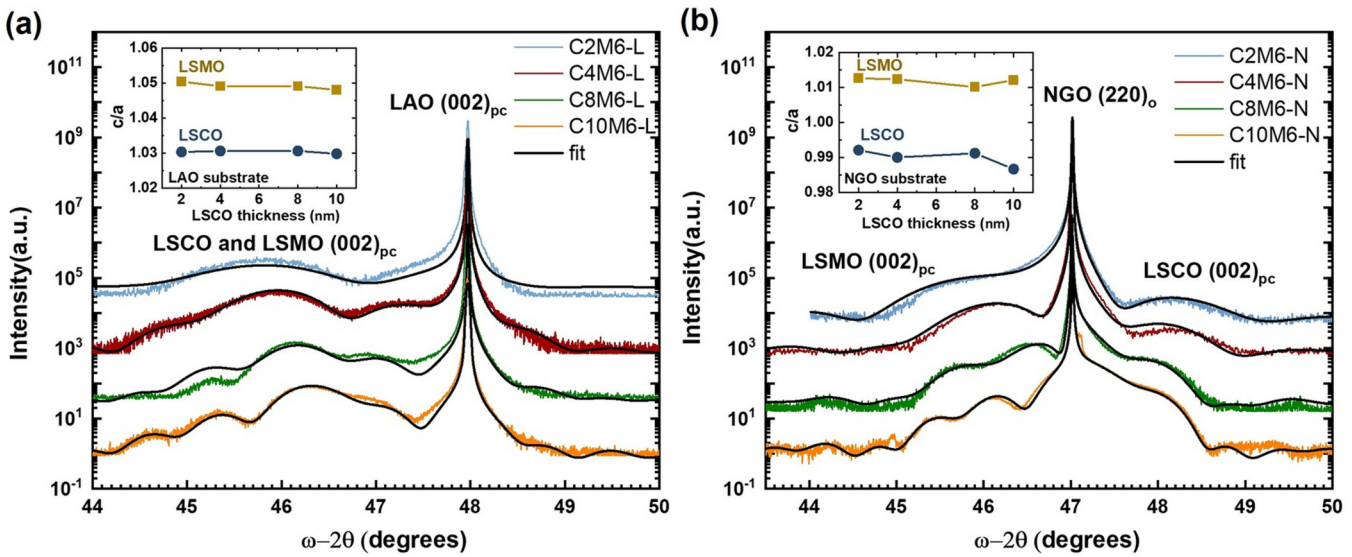

FIG. 2. XRD ω–2θ scans of bilayers on (a) LAO substrates and (b) NGO substrates. Fit curves are shown in black. Curves are vertically shifted for clarity. The inset figures show *c/a* ratios of the LSCO and LSMO layers vs t_{LSCO}.

The LSCO/LSMO bilayers grown on NGO substrates [Fig. 3(b)] display a different trend in their magnetic properties with increasing LSCO thickness. Bilayers C2M6-N and C4M6-N show a single magnetic switching event with almost identical hysteresis loops with large loop squareness ($M_r/M_s = 0.86$) despite the difference in LSCO thickness. This result suggests that the two thinner bilayers share the same magnetocrystalline anisotropy. Two magnetic phases with differing H_c values can be observed in the hysteresis loops for the thicker bilayers C8M6-N and C10M6-N, indicating a combination of soft and hard FM phases. The H_c value of the hard phase increases with increasing LSCO thickness. For bilayer C10M6-N, the hard magnetic switching event at 0.5 T corresponds well with the coercivity of single-layer LSCO films with comparable thickness,[31] while for bilayer C8M6-N, H_c(LSCO) is only slightly larger than H_c(LSMO). It should be noted that bilayers C8M6-N and C10M6-N share a common value of areal M_s, despite the difference in the LSCO thickness.

Magnetization vs temperature ($M(T)$) curves of bilayers on LAO substrates are shown in Fig. 3(c). These curves were measured upon warming in an applied magnetic field of 800 Oe after field cooling at 800 Oe and the Curie temperature (T_c) was determined from the $M(T)$ curves at the peak in dM/dT. The relationship between T_c and LSCO thickness for bilayers on LAO substrates is plotted in Fig. 3(d). Despite the fact that distinct chemical and magnetic layers were confirmed (as discussed further below), only one dominant T_c value can be determined from the $M(T)$ curves.

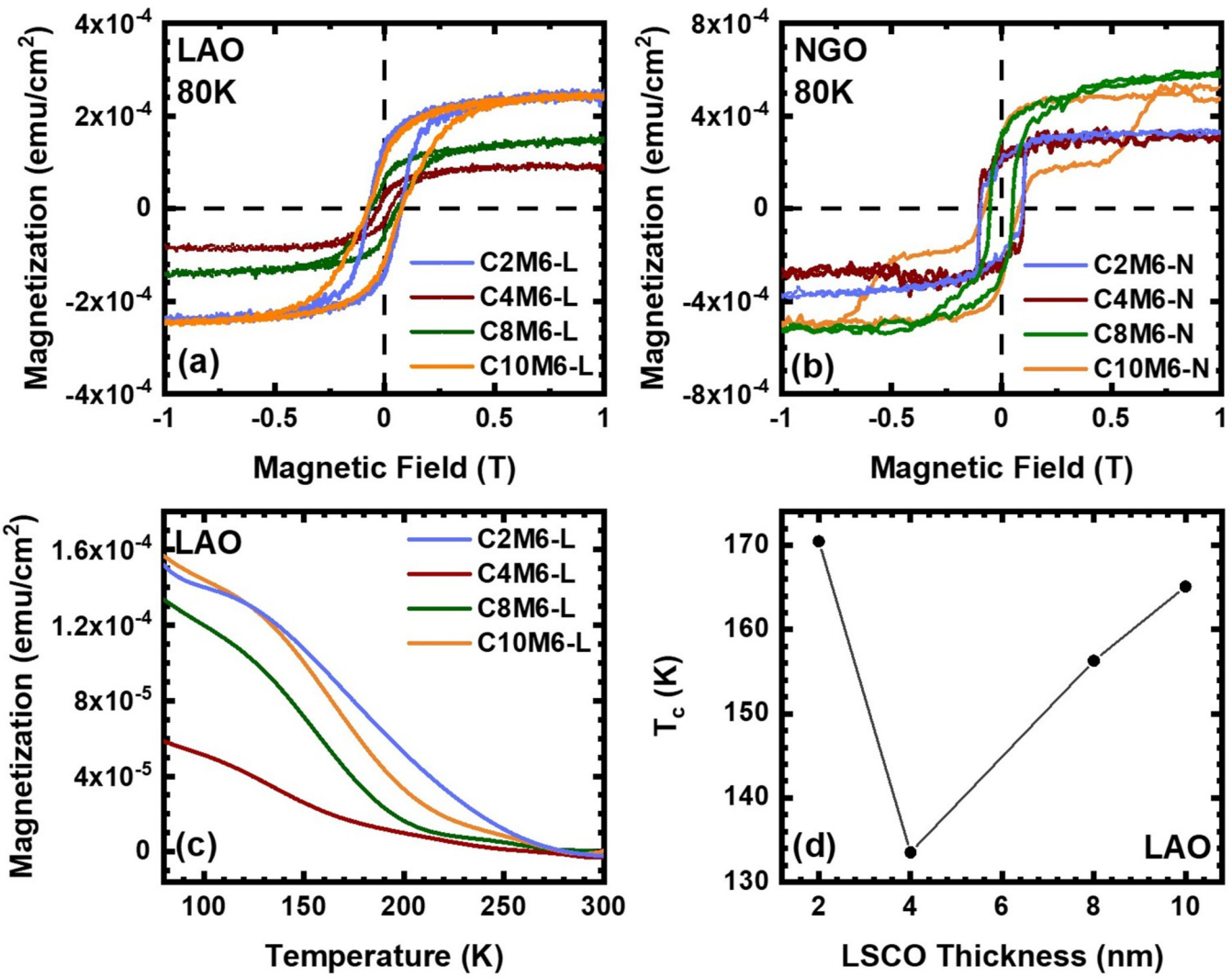

FIG. 3. Magnetic hysteresis loops for LSCO/LSMO bilayers with varying t_{LSCO} grown on (a) LAO and (b) NGO substrates. (c). $M(T)$ curves for bilayers on LAO substrates upon the warming process after 800 Oe field cooling. (d). Curie temperature as a function of t_{LSCO} for bilayers on LAO substrates.

This behavior may result from to the large magnetic field (H = 800 Oe) used to align the hard LSCO sublayers upon warming.[32] Interestingly, bilayer C2M6-L shows the largest T_c value despite having the thinnest LSCO thickness, which suggest different interfacial phenomena from the thicker bilayers. For thicker bilayers, an increasing trend of T_c values can be seen, following the trend of literature results for $La_{0.5}Sr_{0.5}CoO_3$ thin films.[11] These T_c values for the LSCO/LSMO bilayers are lower than the values for bulk LSCO[33] and LSMO.[34] Due to the large paramagnetic signal of the NGO substrates, T_c values were not acquired for those bilayers.

C. Soft x-ray magnetic spectroscopy

To further investigate the origin of the different magnetic characteristics of the LSCO/LSMO bilayers on LAO and NGO substrates, Co/Mn *L*-edge XA/XMCD measurements were performed. From these measurements, information about the valence states and bonding configurations of individual transition metal ions can be obtained. Figures 4(a) and 4(c) compare Co *L*-edge XA spectra of bilayers on LAO and NGO substrates in the TEY mode. The TEY mode is most sensitive to the top 5–10 nm of the sample surface, therefore primarily probes the Co ions at the LSCO/LSMO interface as the signal from the bottom LSCO layer is exponentially diminished. Reference spectra from $CoFe_2O_4$, $LaCoO_3$ and a single-layer (8 nm) LSCO film (C8-L and C8-N) were plotted for comparison to Co^{2+} ions, Co^{3+} ions, and mixed valence Co^{3+}/Co^{4+} ions, all in octahedral coordination. A magnetic $LaCoO_3$ spectra was used as a reference because epitaxial $LaCoO_3$ thin films display ferromagnetic properties at 80 K when Co^{3+} ions are primarily in the intermediate-spin state.[35,36] Labels A, B, and C denote prominent features in the Co^{2+} ion reference spectra and label D marks the Co-L_3 peak position of LSCO reference spectra. Thicker bilayers (LSCO ≥ 4 nm) grown on LAO substrates have almost the same XA curve shape and peak positions [Fig. 4(a)], indicating similar a Co ion valence state and bonding configuration regardless of LSCO thickness. Furthermore, these XA curves show only subtle differences from the single-layer LSCO reference curve (C8-L), suggesting that the Co ions are predominantly in mixed Co^{3+}/Co^{4+} valence states. Bilayer C2M6-L displays prominent spectral features associated with Co^{2+} ions (labeled as features A–C). However, the Co-XA spectra measured in the LY mode [see Fig. S3(a) in the supplementary material] show that bilayer C2M6-L more closely resembles the LSCO reference spectra, suggesting that the Co^{2+} ions are located at the LSCO/LSMO interface, while the mixed Co^{3+}/Co^{4+} ions are closer to the substrate interface. For bilayers on NGO substrates, a similar trend is observed however, the transition from predominantly Co^{2+} ions to mixed Co^{3+}/Co^{4+} ions occurred for the LSCO thickness above 4 nm, a value which approaches the critical thickness (~8 nm) for bilayers grown on LSAT substrates.[15,16]

The shapes of XA spectra depend on the surrounding crystal field[37] as well as spin and valence states.[38] A linear combination of the Co^{2+}, Co^{3+} and mixed Co^{3+}/Co^{4+} ions reference spectra was used as a first order approximation to simulate the experimental Co *L*-edge XA spectra for a discussion of the valence states of Co ions [see Fig. S3 (LY mode) and S4 (TEY mode) in the supplementary material]. The fitting coefficients of the reference spectra vs LSCO thickness are plotted in Fig. S5 in the supplementary material. For the bilayers grown on LAO and NGO substrates, a few general trends can be observed: (1) the LY spectra consistently show a higher proportion of Co^{3+} ions compared to the TEY spectra, suggesting that these Co^{3+} ions reside primarily at the LSCO/substrate interface; (2) the proportion of Co^{3+} ions is consistently higher for the bilayers grown on LAO substrates compared to NGO substrates; (3) both TEY and LY spectra show a trade-off between the concentration of Co^{2+} ions and mixed Co^{3+}/Co^{4+} ions with increasing LSCO thickness; and (4) the TEY spectra show that the Co^{2+} ions in the thinner bilayers are predominantly located at the LSCO/LSMO interface.

The Co-XMCD spectra [Figs. 4(b) and 4(d)] highlight the magnetically active Co ions in the bilayers. Label E denotes the maximum intensity of the Co^{2+} reference spectra, while label F denotes the peak in the Co^{3+}/Co^{4+} ion reference spectra. For the spectra of bilayers (except for C2M6-L) grown on LAO substrates and C8-L reference spectra [Fig. 3(b)], the intensities are multiplied by a factor of 3 to show the features more clearly. The thicker bilayers on both LAO and NGO substrates closely resemble the shape of single-layer LSCO reference spectra, indicating that the magnetically active ions are in a mixed Co^{3+}/Co^{4+} state, while the thinner ones are similar to the Co^{2+} reference spectra. Moreover, the XMCD signal of Co^{2+} ions is much stronger than mixed Co^{3+}/Co^{4+} ions, which can be explained by the high spin state of Co^{2+} in octahedral coordination.[17,39] This result is consistent with our previous studies on LSCO/LSMO bilayers on LSAT substrates which showed that the interfacial Co^{2+} ions have larger magnetization than that of bulk LSCO when the LSCO thickness is below a critical value.[17] This fact also supports the result of the hysteresis loops shown in Fig. 3(a) where bilayer C2M6-L has almost the same areal M_s as bilayer C10M6-L (similarly, C2M6-N has almost the same areal M_s as bilayer C4M6-N). The presence of oxygen vacancies has been reported in $La_{1-x}Sr_xCoO_{3-\delta}$ thin films grown on NGO and LAO substrates,[8,9,40] and as a consequence can lead to the formation of magnetically active Co^{2+} ions with larger ionic radii.[17] The c-lattice expansion observed in Fig. 2 can be explained by the existence of these Co^{2+} ions. The TEY Co-XMCD fitting coefficients [see Fig. S6 in the supplementary material] show a step-like LSCO thickness dependence with magnetic Co^{2+} ions dominating for LSCO thickness ≤2 nm for LAO substrate (LSCO ≤ 4 nm for NGO substrate), becoming mixed Co^{3+}/Co^{4+} ions in the thicker bilayers. In addition, no magnetic contribution from Co^{3+} ions was found regardless of LSCO thickness and substrate type. Combining with the fact from XA spectra fitting results [see Fig. S5 in the supplementary material] that Co^{3+} ions exist at the LSCO/substrate interface, we suggest the existence of a non-magnetic layer at the LSCO/substrate interface due to magneto-electronic phase separation (MEPS).[31,41,42] The thickness of this MEPS layer was found to be below 2.3 nm for $La_{0.5}Sr_{0.5}CoO_3$ films on LAO substrates[9] and it increased with decreasing Sr-doping and increasing epitaxial strain.[31,41] The fact that robust magnetic properties are observed for bilayers with LSCO thicknesses below this critical thickness for MEPS suggests that the formation of Co^{2+} ions at the LSCO/LSMO interface is able to overpower MEPS at the LSCO/substrate interface. Furthermore, this MEPS layer can explain the larger proportion of Co^{3+} ions observed for the bilayer on LAO substrates where the LSCO layer exists under a −1% compressive strain.

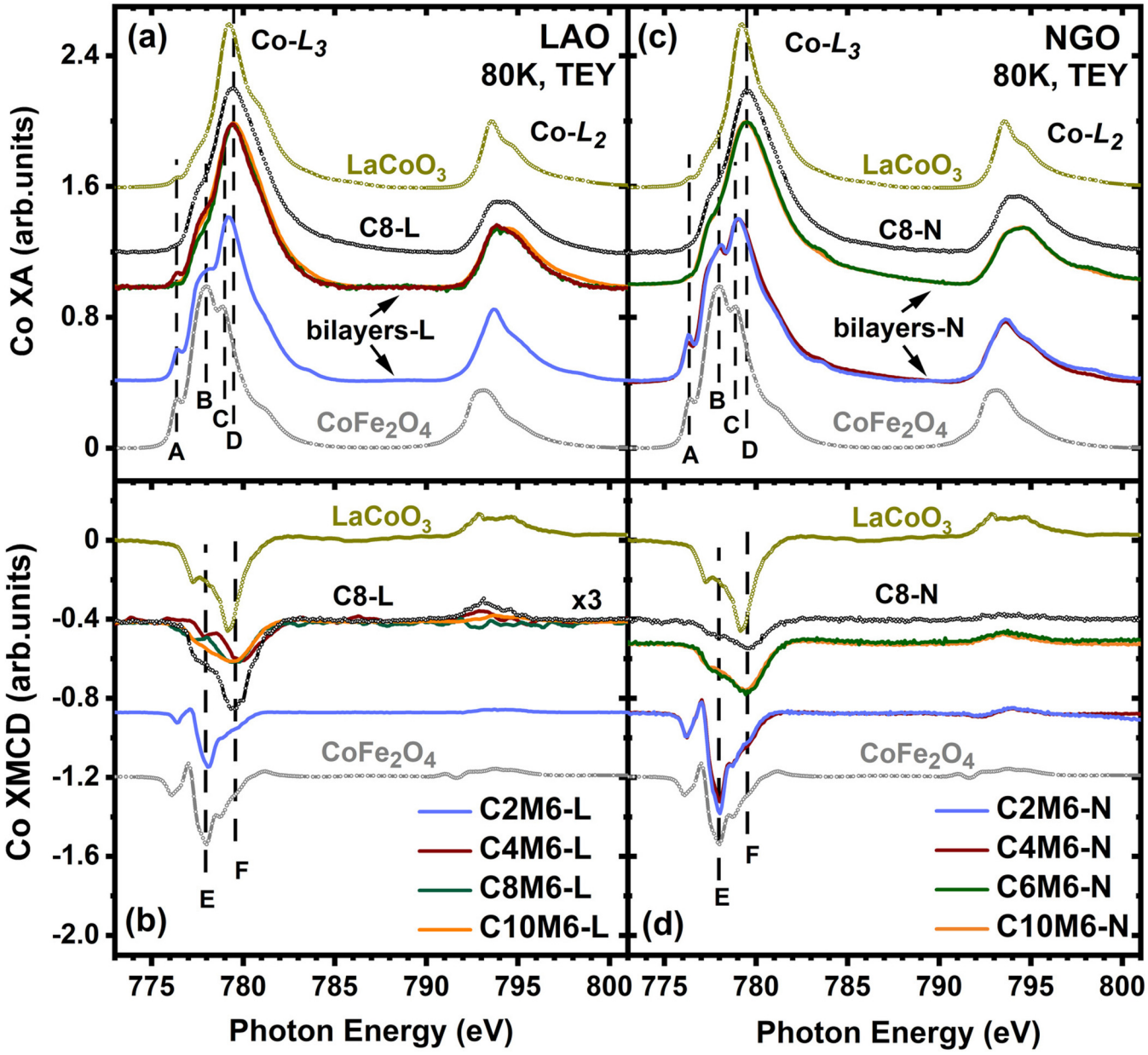

FIG. 4. Co *L*-edge XA/XMCD spectra of (a) and (b) bilayers on LAO substrates and (c) and (d) bilayers on NGO substrates taken in the TEY mode (interfacial region). Labels A–F denote prominent spectral features. Thicker bilayers and C8-L in (b) are multiplied by a factor of 3. XA/XMCD spectra are normalized to the L_3-edge average XA peak and are vertically shifted for clarity. Reference spectra for LSCO (8 nm), $LaCoO_3$, and $CoFe_2O_4$ thin films taken in the TEY mode are included for comparison.

As with previous studies of LSCO/LSMO bilayers grown on LSAT substrates,[15,16] the Mn XA/XMCD spectral shapes and intensities for the bilayers on NGO substrates [Figs. 5(c) and 5(d)] showed only subtle differences with increasing LSCO layer thickness and the curves matched well with single-layer LSMO films. However, the bilayers on LAO substrates [Figs. 5(a) and 5(b)] displayed minor deviations from the behavior observed on NGO and LSAT substrates. Figure 5 shows the Mn L_3-edge XA/XMCD only to clearly compare the spectral features. Labels A and B in Fig. 5 denote prominent features on the Mn-L_3 edge XA spectra. Full range normalized spectra including Mn L_2-edge are shown in Fig. S8 in the supplementary material. Among all Mn-XA curves in Figs. 5(a) and 5(b), only the thicker bilayers (LSCO > 2 nm) on LAO substrates show the shoulder feature A as well as the shifting

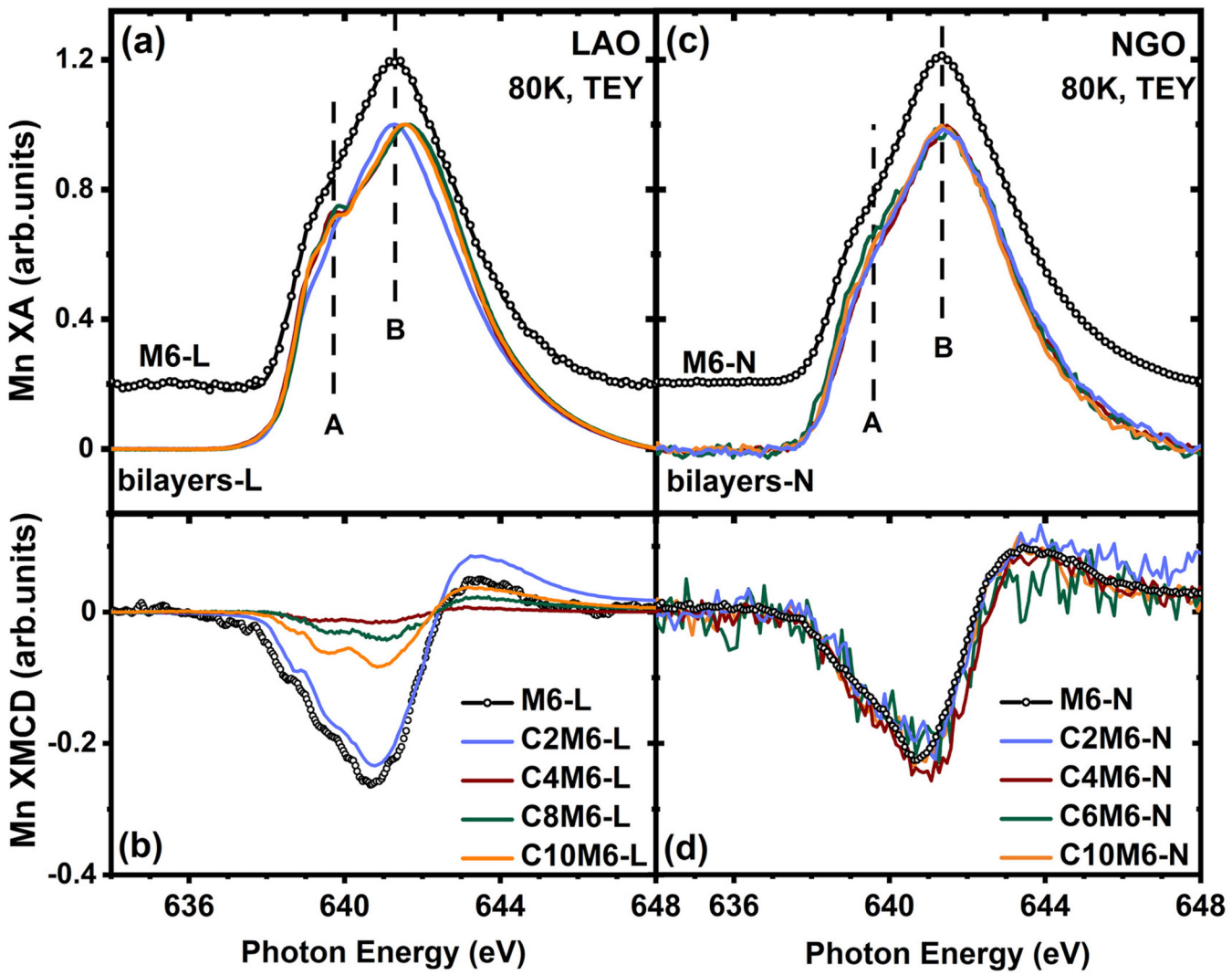

FIG. 5. Mn L_3-edge XA/XMCD spectra of (a) and (b) bilayers on LAO substrate and (c) and (d) bilayers on NGO substrates taken in the TEY mode. Labels A and B mark prominent spectral features. XA/XMCD spectra are normalized to the L_3-edge average XA peak. The M6 XA spectra are vertically shifted for clarity.

of the main peak B to higher photon energy compared to the LSMO reference samples and bilayers on NGO substrates, indicating an increased Mn^{4+} ion concentration.[43] Unlike the bilayers grown on LSAT substrates, where a higher Mn^{4+} ion concentration was observed in the thinner bilayers due to interfacial charge transfer from (Mn^{3+} + Co^{3+}) to (Mn^{4+} + Co^{2+}),[15,16] on LAO substrates the thinnest bilayer (C2M6-L) possessed higher Mn^{3+} concentration along with the presence of Co^{2+} ions. In this case of large compressive strain, one must consider an additional contribution from the formation of oxygen vacancies which lowers the average Mn valence state in ultrathin LSMO films.[44]

This competition between factors such as charge transfer and oxygen vacancy formation leads to a robust Mn-XMCD signal for bilayer C2M6-L. For thicker bilayers on LAO substrates, the Mn-XMCD signal is nearly absent in bilayer C4M6-L and then gradually increases with increasing LSCO layer thickness despite the fact that the LSMO thickness remains fixed at 6 nm. The maximum XMCD intensities remain much lower than that of a single-layer LSMO film and bilayer C2M6-L. Previously, a trend of increasing M_s values for LSMO layers with increasing buffer layer thickness was attributed with decreased structural distortions at the buffer layer/LSMO interface.[12] Similarly, we postulate that the epitaxial strain that builds up with increasing LSCO thickness is accommodated differently on LAO substrates (compared to LSAT and NGO substrates) as all the layers possess the same $a^-a^-a^-$ tilt pattern. A variation of octahedral tilt angles due to oxygen vacancy ordering at the LSCO/LSMO interface could explain the strong thickness dependence observed in the magnetic properties of the

LSMO layer. It has been reported that the oxygen vacancy ordering directions are different when $La_{0.5}Sr_{0.5}CoO_3$ film is under tensile vs compressive strain.[9,45] Additional characterization, such as scanning transmission electron microscopy, will be required to quantify these differences but is outside the scope of the current work.

D. XMCD hysteresis loops

Finally, Co- and Mn-edge XMCD loops of the LSCO/LSMO bilayers on LAO substrates [Fig. 6] allow us to distinguish between the magnetic contributions from the two FM layers on LAO substrates, The XMCD loops were measured at specific Co/Mn-edge energies which correspond to the maximum in the XMCD spectra. Both hysteresis loops for bilayer C2M6-L [Fig. 6(a)] are almost identical, indicating that the two layers are fully coupled. For thicker bilayers, the Co and Mn XMCD loops indicate that the LSCO and LSMO layers are indeed switching independently, despite the fact that the VSM bulk hysteresis loops [Fig. 3(a)] do not show distinct magnetic switching events. Figure S8 in the supplementary material shows that the VSM hysteresis loop for bilayer C8M6-L (red dots) can be reproduced using a linear fit of the Co-/Mn-XMCD hysteresis loops (black curve) with a Co: Mn = 1:1.8 ratio of fitting coefficients. This ratio agrees well with the magnetization ratio (LSCO : LSMO = 1:1.5) obtained from single-layer LSCO (C8-L) and LSMO (M6-L) films in Fig. S1 in the supplementary material. Co-/Mn-XMCD hysteresis loops clearly show that the H_c values increase with increasing LSCO thickness but remain below that of bilayers on NGO substrates [Fig. 3(a)].

The combination of XA/XMCD spectra and magnetic hysteresis loops suggests that both epitaxial strain and LSCO thickness

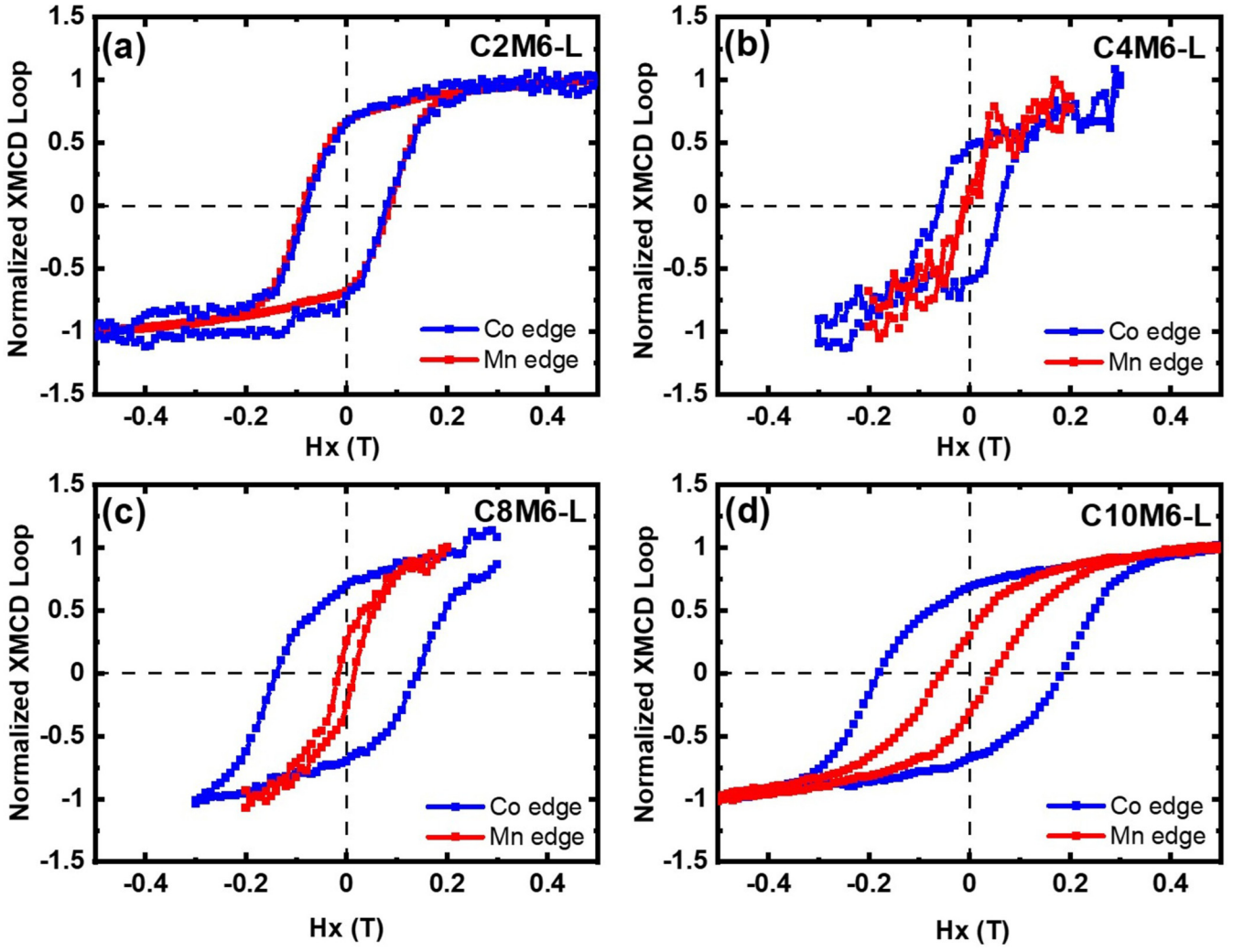

FIG. 6. Normalized Co and Mn *L*-edge XMCD loops of LSCO/LSMO bilayers on LAO substrates. The hysteresis loops were measured at specific Co/Mn-edge energies which correspond to the maximum in the XMCD spectra.

strongly influence the formation of magnetic layers in the LSCO/LSMO bilayer system [see the inset tof Fig. 7], and that interfacial charge transfer alone cannot fully explain the behavior. The bilayers grown on LAO substrates exist under large compressive strain and share the same bulk octahedral tilt patterns as the substrate but with differing tilt angles. In this case, the LY XA/XMCD measurements suggest the presence of a MEPS LSCO layer consisting primarily of non-magnetic Co^{3+} ions at the LAO interface. TEY measurements demonstrate that the magnetic properties of the remainder of the LSCO layer as well as the LSMO layer depend strongly on LSCO thickness. For bilayer C2M6-L, Co^{2+} ions [red triangles in Fig. 7] at the LSCO/LSMO interface couple magnetically to the LSMO layer. The comparatively large M_s [shown in Fig. 3(a) and triangles in Fig. 7(c)] comes from robust magnetization of both LSCO and LSMO layers. For LSCO thicknesses from 4 to 10 nm, the concentration of Co^{2+} ions is rapidly suppressed as the LSCO thickness increases, leading to a soft LSCO layer characterized by mixed valence Co^{3+}/Co^{4+} ions [blue triangles in Fig. 7]. The LSCO and LSMO layers switch independently of one another and their coercivity and magnetization values increase gradually with LSCO thickness, though even at a LSCO thickness of 10 nm, their M_s values remain suppressed below that of single-layer LSCO and LSMO films on LAO substrates. Therefore, for bilayers under compressive strain, the magnetic properties of both LSCO and LSMO layers displayed a strong LSCO thickness dependence.

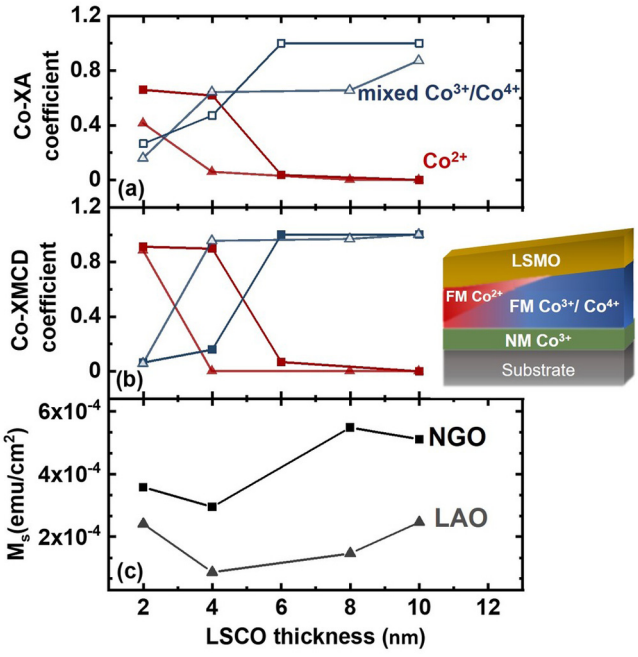

FIG. 7. (a) Co-XA fitting coefficients and (b) Co-XMCD fitting coefficients vs t_{LSCO} of bilayers on LAO (triangle) and NGO (square) substrates. Blue lines are for mixed valence Co^{3+}/Co^{4+} ions. Red lines are for Co^{2+} ions. (c). Areal M_s vs t_{LSCO} of LSCO/LSMO bilayers. The inset figure shows the distribution of Co ions in the bilayers as t_{LSCO} increases (from left to right).

The bilayers grown on NGO substrates exist under mixed compressive and tensile strain and their bulk octahedral tilt patterns differ from the substrate. Though a similar evolution of Co^{2+} ions to mixed valence Co^{3+}/Co^{4+} ions [see Fig. 7, square symbols] was found, the critical LSCO thickness was 4 nm and the magnetic properties of the LSMO layer was largely unaffected by the change in LSCO thickness. This thickness-dependent LSCO magnetic structure is more abrupt than that found previously in bilayers on LSAT substrates, despite of the fact that the strain of the bilayers remains approximately the same on both substrates.[15,16] Therefore, we can conclude that both epitaxial strain and octahedral tilt patterns affect the magnetic properties of LSCO/LSMO bilayers, but the impact of compressive strain (when LSCO/LSMO bilayers are on LAO substrates) is more pronounced and advanced structural characterization will be needed to quantify the octahedral tilt angles and any oxygen vacancy ordering that may be induced by the epitaxial strain state.

IV. CONCLUSION

In summary, we investigated the strain- and thickness-dependent magnetic properties of LSCO/LSMO bilayers grown on LAO and NGO substrates. The combination of soft x-ray magnetic spectroscopy and bulk magnetometry allowed us to explore their electronic and magnetic structures. For bilayers on both LAO and NGO substrates, a non-magnetic layer characterized by Co^{3+} ions exists at the LSCO/substrate interface at thicknesses below 2 nm. As was previously found in bilayers grown on LSAT substrates, the bilayers on NGO substrates with LSCO thickness $\leq$4 nm showed the formation of a soft LSCO layer at the LSCO/LSMO interface characterized by magnetically active Co^{2+} ions which couple magnetically to the soft LSMO layer. With increasing LSCO thickness to 6–10 nm, the formation of the Co^{2+} ions was quickly suppressed leaving only a hard LSCO layer with mixed valence Co^{3+}/Co^{4+} ions. However, the magnetic properties of the LSMO layer were independent of the LSCO thickness and no Mn^{4+} ions were observed. In contrast, the magnetic properties of both LSCO and LSMO layers displayed a strong LSCO thickness dependence when grown on LAO substrates. The magnetically active Co^{2+} ions predominate in the bilayer with LSCO thickness = 2 nm. The strong FM signal from Co^{2+} ions and Mn ions lead to the relatively larger M_s values compare to other bilayers on LAO substrates. An increasing trend of areal M_s values can be observed as LSCO thickness increasing from 4 to 10 nm, which follows the similar trend of increasing FM signal of Mn ions. The differences in the magnetic and electronic properties in these bilayers cannot be explained solely based on interfacial charge transfer and likely arise from subtle structure changes resulting from factors such as epitaxial strain states, oxygen vacancies, and octahedral tilts. These findings provide a path to tune the functional properties of complex oxide heterostructures and develop a fundamental understanding of interfacial exchange spring behavior needed for their implementation in next generation spintronic and magnetic memory devices.

SUPPLEMENTARY MATERIAL

See the supplementary material for VSM bulk magnetic hysteresis loops of single-layer LSCO and LSMO, fitting results of

XA/XMCD spectra and VSM bulk magnetic hysteresis loop fitting results.

ACKNOWLEDGMENTS

Financial support for this project was provided by the National Science Foundation grant DMR—No. 1745450. This research used resources of the Advanced Light Source, which is a U.S. Department of Energy (DOE) Office of Science User Facility under Contract No. DE-AC02-05CH11231, Use of the Stanford Synchrotron Radiation Lightsource, SLAC National Accelerator Laboratory, is supported by the U.S. DOE, Office of Science, Office of Basic Energy Sciences under Contract No. DE-AC02-76SF00515.

AUTHOR DECLARATIONS

Conflict of Interest

The authors have no conflicts to disclose.

Author Contributions

Mingzhen Feng: Data curation (equal); Formal analysis (equal); Methodology (equal); Software (equal); Writing – original draft (equal); Writing – review & editing (equal). **Nolan J. Ahlm:** Data curation (equal); Formal analysis (equal); Methodology (equal). **Alexander M. Kane:** Data curation (equal); Formal analysis (equal); Resources (equal). **I-Ting Chiu:** Data curation (equal); Formal analysis (equal); Resources (equal). **Dayne Y. Sasaki:** Data curation (equal); Formal analysis (equal); Resources (equal). **Padraic Shafer:** Data curation (supporting); Resources (equal); Software (equal); Writing – review & editing (supporting). **Alpha T. N'Diaye:** Data curation (supporting); Resources (supporting); Software (supporting). **Apurva Mehta:** Data curation (supporting); Resources (supporting); Software (supporting). **Yayoi Takamura:** Conceptualization (equal); Funding acquisition (lead); Investigation (lead); Supervision (lead); Writing – review & editing (equal).

DEDICATION

M.F. wishes to thank Y. Takamura for great support and guidance on this project with her rich knowledge and accomplishment in growth and characterizations of complex oxide thin films.

DATA AVAILABILITY

The data that support the findings of this study are available from the corresponding author upon reasonable request.

REFERENCES

[1]S. Gariglio, M. Gabay, and J. M. Triscone, APL Mater. **4**, 060701 (2016).
[2]A. J. Millis, T. Darling, and A. Migliori, J. Appl. Phys. **83**, 1588 (1998).
[3]M. Imada, A. Fujimori, and Y. Tokura, Rev. Mod. Phys. **70**, 1039 (1998).
[4]P. Zubko, S. Gariglio, M. Gabay, P. Ghosez, and J.-M. Triscone, Annu. Rev. Condens. Matter Phys. **2**, 141 (2011).
[5]M. Bibes, J. E. Villegas, and A. Barthélémy, Adv. Phys. **60**, 5 (2011).
[6]A. M. Haghiri-Gosnet, J. Wolfman, B. Mercey, C. Simon, P. Lecoeur, M. Korzenski, M. Hervieu, R. Desfeux, and G. Baldinozzi, J. Appl. Phys. **88**, 4257 (2000).
[7]F. Tsui, M. C. Smoak, T. K. Nath, and C. B. Eom, Appl. Phys. Lett. **76**, 2421 (2000).
[8]M. D. Biegalski, Y. Takamura, A. Mehta, Z. Gai, S. V. Kalinin, H. Ambaye, V. Lauter, D. Fong, S. T. Pantelides, Y. M. Kim, J. He, A. Borisevich, W. Siemons, and H. M. Christen, Adv. Mater. Interfaces **1**, 1400203 (2014).
[9]J. Walter, S. Bose, M. Cabero, G. Yu, M. Greven, M. Varela, and C. Leighton, Phys. Rev. Mater. **2**, 111404(R) (2018).
[10]J. P. Byers, B. Li, R. V. Chopdekar, J. Ditto, D. C. Johnson, Y. Takamura, and N. D. Browning, J. Appl. Phys. **125**, 082518 (2019).
[11]C. Xie, J. I. Budnick, B. O. Wells, and J. C. Woicik, Appl. Phys. Lett. **91**, 172509 (2007).
[12]Z. Liao, M. Huijben, Z. Zhong, N. Gauquelin, S. Macke, R. J. Green, S. Van Aert, J. Verbeeck, G. Van Tendeloo, K. Held, G. A. Sawatzky, G. Koster, and G. Rijnders, Nat. Mater. **15**, 425 (2016).
[13]D. Kan, R. Aso, R. Sato, M. Haruta, H. Kurata, and Y. Shimakawa, Nat. Mater. **15**, 432 (2016).
[14]B. Li, R. V. Chopdekar, E. Arenholz, A. Mehta, and Y. Takamura, Appl. Phys. Lett. **105**, 202401 (2014).
[15]B. Li, R. V. Chopdekar, A. T. N'Diaye, A. Mehta, J. P. Byers, N. D. Browning, E. Arenholz, and Y. Takamura, Appl. Phys. Lett. **109**, 152401 (2016).
[16]A. M. Kane, R. V. Chopdekar, A. T. N'Diaye, A. Scholl, E. Arenholz, A. Mehta, and Y. Takamura, Phys. Rev. Mater. **3**, 014413 (2019).
[17]A. M. Kane, I. T. Chiu, N. J. Ahlm, R. V. Chopdekar, A. T. N'diaye, E. Arenholz, A. Mehta, V. Lauter, and Y. Takamura, ACS Appl. Mater. Interfaces **12**, 45437 (2020).
[18]A. M. Glazer, Acta Crystallogr. Sect. B Struct. Crystallogr. Cryst. Chem. **28**, 3384 (1972).
[19]L. Vasylechko, L. Akselrud, W. Morgenroth, U. Bismayer, A. Matkovskii, and D. Savytskii, J. Alloys Compd. **297**, 46 (2000).
[20]T. T. Fister, H. Zhou, Z. Luo, S. S. A. Seo, S. O. Hruszkewycz, D. L. Proffit, J. A. Eastman, P. H. Fuoss, P. M. Baldo, H. N. Lee, and D. D. Fong, APL Mater. **2**, 021102 (2014).
[21]I. Hallsteinsen, M. Moreau, A. Grutter, M. Nord, P. E. Vullum, D. A. Gilbert, T. Bolstad, J. K. Grepstad, R. Holmestad, S. M. Selbach, A. T. N'Diaye, B. J. Kirby, E. Arenholz, and T. Tybell, Phys. Rev. B **94**, 201115 (2016).
[22]N. Kemik, M. Gu, F. Yang, C. Y. Chang, Y. Song, M. Bibee, A. Mehta, M. D. Biegalski, H. M. Christen, N. D. Browning, and Y. Takamura, Appl. Phys. Lett. **99**, 201908 (2011).
[23]M. Björck and G. Andersson, J. Appl. Crystallogr. **40**, 1174 (2007).
[24]A. Ulyanenkov, Proc. SPIE **5536**, 1 (2004).
[25]A. R. Dzhanoev, F. Spahn, V. Yaroshenko, H. Lühr, and J. Schmidt, Phys. Rev. B **92**, 125430 (2015).
[26]A. Bianconi, D. Jackson, and K. Monahan, Phys. Rev. B **17**, 2021 (1978).
[27]G. van der Laan and A. I. Figueroa, Coord. Chem. Rev. **277–278**, 95 (2014).
[28]E. Arenholz, private communication (2015).
[29]C. H. Kim, J. W. Jang, S. Y. Cho, I. T. Kim, and K. S. Hong, Phys. B **262**, 438 (1999).
[30]J. Z. Sun, D. W. Abraham, R. A. Rao, and C. B. Eom, Appl. Phys. Lett. **74**, 3017 (1999).
[31]B. Li, R. V. Chopdekar, A. M. Kane, K. Hoke, A. T. N'Diaye, E. Arenholz, and Y. Takamura, AIP Adv. **7**, 045003 (2017).
[32]R. V. Chopdekar, V. K. Malik, A. M. Kane, A. Mehta, E. Arenholz, and Y. Takamura, J. Phys.: Condens. Matter **30**, 015805 (2018).
[33]J. Wu and C. Leighton, Phys. Rev. B **67**, 174408 (2003).
[34]C. Adamo, X. Ke, H. Q. Wang, H. L. Xin, T. Heeg, M. E. Hawley, W. Zander, J. Schubert, P. Schiffer, D. A. Muller, L. Maritato, and D. G. Schlom, Appl. Phys. Lett. **95**, 112504 (2009).
[35]M. A. Korotin, S. Y. Ezhov, I. V. Solovyev, V. I. Anisimov, D. I. Khomskii, and G. A. Sawatzky, Phys. Rev. B **54**, 5309 (1996).
[36]D. Fuchs, E. Arac, C. Pinta, S. Schuppler, R. Schneider, and H. V. Löhneysen, Phys. Rev. B **77**, 014434 (2008).
[37]A. Grimaud, C. E. Carlton, M. Risch, W. T. Hong, K. J. May, and Y. Shao-Horn, J. Phys. Chem. C **117**, 25926 (2013).

[38]M. Merz, P. Nagel, C. Pinta, A. Samartsev, H. V. Löhneysen, M. Wissinger, S. Uebe, A. Assmann, D. Fuchs, and S. Schuppler, Phys. Rev. B **82**, 174416 (2010).
[39]C. F. Chang, Z. Hu, H. Wu, T. Burnus, N. Hollmann, M. Benomar, T. Lorenz, A. Tanaka, H. J. Lin, H. H. Hsieh, C. T. Chen, and L. H. Tjeng, Phys. Rev. Lett. **102**, 116401 (2009).
[40]J. Gazquez, S. Bose, M. Sharma, M. A. Torija, S. J. Pennycook, C. Leighton, and M. Varela, APL Mater. **1**, 012105 (2013).
[41]M. A. Torija, M. Sharma, J. Gazquez, M. Varela, C. He, J. Schmitt, J. A. Borchers, M. Laver, S. El-Khatib, and C. Leighton, Adv. Mater. **23**, 2711 (2011).
[42]M. Sharma, J. Gazquez, M. Varela, J. Schmitt, and C. Leighton, Phys. Rev. B **84**, 024417 (2011).
[43]G. Shibata, K. Yoshimatsu, E. Sakai, V. R. Singh, V. K. Verma, K. Ishigami, T. Harano, T. Kadono, Y. Takeda, T. Okane, Y. Saitoh, H. Yamagami, A. Sawa, H. Kumigashira, M. Oshima, T. Koide, and A. Fujimori, Phys. Rev. B **89**, 235123 (2014).
[44]B. Cui, C. Song, F. Li, G. Y. Wang, H. J. Mao, J. J. Peng, F. Zeng, and F. Pan, Sci. Rep. **4**, 4206 (2015).
[45]X. Rui and R. F. Klie, Appl. Phys. Lett. **114**, 233101 (2019).